An Enhanced Sensor Deployment Scheme for Automated Smart Environments[†]

Ting-Yu Lin[⋆], Hendro Agus Santoso, Wei-Ting Liu, and Huan-Ting Liu
Department of Electrical and Computer Engineering
National Chiao Tung University

Abstract—For the wireless sensor network (WSN) to operate successfully, a critical issue is to provide sufficient sensing coverage. In this paper, we target on smart environments and deal with both the homogeneous (having identical sensing radius) and heterogeneous sensors (having different sensing ranges) equipped with locomotion facilities to assist in the sensor self-deployment. An enhanced virtual forces algorithm with boundary forces (EVFA-B) protocol is proposed to realize an automated monitoring network. The EVFA-B mechanism exerts weighted attractive and repulsive forces on each sensor based on predefined distance thresholds. Resultant forces then guide the sensors to their suitable positions with the objective of enhancing the sensing coverage (after a possibly random placement of sensors). To achieve high coverage ratio, we infer that good choices for the associated weight constants greatly depend on sensor population and monitored area size, while independent of sensing radius. Performance of the proposed sensor deployment strategy is evaluated in terms of surveillance coverage and moving energy consumption. We also implement our EVFA-B deployment mechanism in a real-life monitoring network (MoNet) to demonstrate the protocol feasibility.

I. INTRODUCTION

Advances of micro-electromechanical system (MEMS), sensing technology, and wireless communication have significantly encouraged the development of wireless sensor networks (WSNs) in the past decade. A WSN is widely used for habitat and environmental surveillance, medical application (with the purpose of improving quality of health care), agricultural assistance, and as solutions to military problems [10], [11]. Several experimental testbeds are also implemented to investigate various aspects of WSN-related performance issues [7], [12], [13]. Since different environments usually guide WSN studies to distinct research directions and design considerations, it is necessary to firstly define the target environment under investigation. In this paper, we focus on the indoor smart environment, as depicted in Fig. 1. To furnish the environment with monitoring capability, one possibility could be embedding a secret compartment under the roof, and deploying smart sensors inside the double-deck structure on the ceiling. For a successful surveillance, providing sufficient sensing coverage is essential. Manual placement of static sensors involves labor effort to reach the ceiling for performing a planned deployment. Thanks to the availability of motion facilities, we consider smart sensors with mobility capability to accomplish
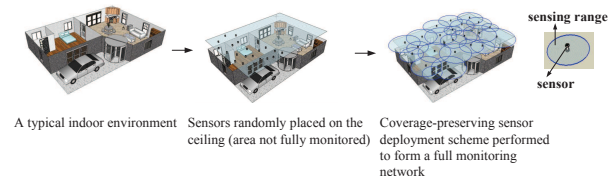
Fig. 1.   Illustration of an automated monitoring network.

self-deployment after an initial random placement of sensors, and propose an enhanced sensor deployment scheme to ensure sufficient sensing coverage. In this work, we do ***not*** intend to study the energy-conserving sensor communication behavior (though we try to reduce the moving energy by keeping sensors from moving far away when performing self-deployment), ***nor*** the issue of required amount of sensors to achieve certain degree of sensing coverage. Rather, given any number of sensors, we investigate the deployment problem and develop a coverage-aware sensor deployment protocol based on the concept of virtual forces in a bounded monitoring area, with the objective of providing/maintaining high sensing coverage. Our ultimate goal is to realize an automated monitoring network so that detection applications of various emergency events can be practically implemented.

The remainder of this paper is organized as follows. Section II reviews several prior research efforts and summarizes our unique contributions. In Section III, we provide the environmental assumptions made by the protocol. Section IV elaborates on the detailed operations of proposed EVFA-B deployment scheme. Section V presents the performance comparison results, and briefly reports our prototype of an automated monitoring network (MoNet). Finally, we draw our concluding remarks in Section VI.

II. PRIOR WORK AND OUR CONTRIBUTIONS

Depending on the target applications, earlier studies in WSNs generally focus on either outdoor large-scale environments, where planned sensor deployment is difficult, or indoor small-scale monitoring zones, where sensor deployment mechanism is feasible and beneficial. For large-scale WSNs, several works have been proposed to address the energy conservation issue [9], [15], [17]. For the monitoring environments where planned sensor deployment is possible, various static deployment strategies have been introduced to enhance the surveillance coverage [5], [8]. However, such static deployment involves manual sensor placement/installation, and is incapable of dynamically repairing sensing voids (uncovered

areas) in the presence of unexpected sensor failures. Consequently, a number of research efforts have explored the movement-assisted sensor deployment techniques by utilizing mobile sensors to enhance the sensing coverage after an initial random placement of sensors [14], [16], [18]. Those deployment techniques all consider homogeneous sensors (having equal sensing/detection radius). With the motion facilities equipped at the sensing devices, sensors can move around to deploy themselves.

We summarize our unique contributions made in this paper as follows. First, *we develop an enhanced virtual forces algorithm with boundary forces (EVFA-B) based on the concept of potential field and disk packing theory*. Though sharing similar idea of virtual forces with [18], our EVFA-B deals with both the homogeneous and heterogeneous sensors (with different sensing distances), while [18] only discusses the case of homogeneous sensors, where a global distance threshold value is adopted in determining whether an attractive (with weight constant w_a) or repulsive (with weight constant w_r) force should be applied on a sensor. However, in realistic settings, where varying sensing ranges are common, *the distance threshold (determining the desirable sensing overlapping degree) should be selected on a node-pair basis, instead of being set globally*. In addition, since the observed environment is usually in a bounded area, *our EVFA-B protocol incorporates the boundary force (with weight constant w_b) as a kind of repulsive force from the boundaries to keep sensors staying inside the monitoring area*. Since the boundary force is considered as a type of repulsive force, we use the same value for w_r and w_b. In [18], no boundary force is modeled, and no specific design guidelines are available for determining suitable w_a and w_r (=w_b) weight constants. The authors only suggest to select $w_r >> w_a$. However, we discover that arbitrary settings (even satisfying $w_r >> w_a$) do not always yield desirable sensing coverage. Motivated by the observations, we investigate and conjecture that *good choices for w_a and w_r (=w_b) greatly depend on sensor population and monitored area dimensions, while independent of sensing radius*. Second, we observe that most existing works do not have a real-life testbed to demonstrate their proposed protocols/algorithms. In this work, *we implement an automated monitoring network (MoNet)*, based on embedded platforms, sensing components, communication modules and motion devices, *to validate the proposed EVFA-B protocol*.

III. ENVIRONMENTAL ASSUMPTIONS

Below we summarize the environmental assumptions made in this work.

(A1) There exists a powerful clusterhead responsible for performing centralized computations. All sensors are able to communicate with the clusterhead via single-hop or multi-hop wireless transmissions.

(A2) Sensors have the isotropic sensing shape and the binary sensing/detection behavior, in which an event is detected (not detected) by a sensor with complete certainty if this event occurs inside (outside) its sensing radius. Both the homogeneous (having identical sensing range) and heterogeneous (having varying sensing ranges) sensors are
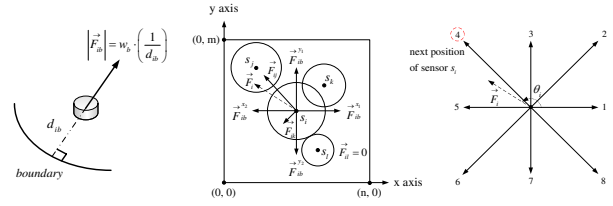

Fig. 2. Concept of attractive, repulsive, boundary forces, and virtual movement exerted on a sensor node.

allowed in our model. Information of respective sensing ranges is provided by all sensors and made available at the clusterhead for deployment-related computations.

(A3) We adopt the discrete coordination system, in which the monitoring area (sensing field) is represented by a 2D grid network. Locations of all sensors are obtained via the pre-deployed RFID platform or some existing localization technique, and constantly updated to the clusterhead. Neighboring nodes under the adopted coordination system are defined as sensors within the sensing range (r_s), which is normally much smaller than the radio communication distance (r_c). Without loss of generality, we assume that $r_c > 2r_s$ in our model. According to the derivations in [9], [17], if the radio communication range (r_c) is at least twice the sensing radius (r_s), complete coverage of a convex area implies connectivity among the working set of sensor nodes. Consequently, in this work, we only deal with the sensing coverage, and network connectivity follows accordingly.

IV. ENHANCED VIRTUAL FORCES ALGORITHM WITH BOUNDARY FORCES (EVFA-B)

The concept of virtual forces is inspired by the combined idea of potential field and disk packing theory [6]. Each sensor behaves as a source giving a force to others. This force can be either positive (attractive) or negative (repulsive). If two sensors are too close, they exert repulsive forces to separate each other, otherwise they exert attractive forces to draw each other. We quantify the definition of "closeness" by using the distance threshold d_{th}^{ij} for any two sensors s_i and s_j with respective sensing radius r_i and r_j (design guidelines on d_{th}^{ij} are provided in Section IV-A). Given k sensors (denoted as s_1, s_2, ..., s_k with sensing radius r_1, r_2, ..., r_k, respectively) deployed in the monitoring area, for any two sensors s_i and s_j located at coordinates (x_i, y_i) and (x_j, y_j), we adopt the Euclidean distance d_{ij} to indicate how far the two sensors are spaced, where $d_{ij} = \sqrt{(x_i - x_j)^2 + (y_i - y_j)^2}$. As a result, if $d_{ij} > d_{th}^{ij}$, then attractive force is applied. On the other hand, repulsive force is generated if $d_{ij} < d_{th}^{ij}$. Define $\overrightarrow{F}_{ij}$ as the directed virtual force acting on s_i from s_j, now we have

$$\overrightarrow{F}_{ij} = \left\{ \begin{array}{ll} (w_a(d_{ij} - d_{th}^{ij}), \theta_{ij}) & \text{for } d_{ij} > d_{th}^{ij} \\ (0, 0) & \text{for } d_{ij}^{ij} = d_{th} \\ (w_r(d_{th}^{ij} - d_{ij}), \theta_{ij} + \pi) & \text{otherwise} \end{array} \right\}, \quad (1)$$

where $\theta_{ij} = \tan^{-1} \frac{(y_i - y_j)}{(x_i - x_j)}$ and w_a (w_r) represents the weight measurement for the attractive (repulsive) force (detailed de-
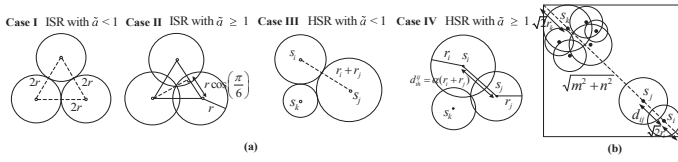
Fig. 3. (a) Distance threshold (d_{th}^{ij}) settings for two arbitrary sensors s_i and s_j under four different environmental conditions. (b) Extreme node configuration used to derive the proper $\frac{w_r}{w_a}$ ratio setting.

sign guidelines on the two weight constants are elaborated in Section IV-B). Take s_i in Fig. 2 for example, attractive force $\overrightarrow{F}_{ij}$ from s_j (to draw s_i closer) and repulsive force $\overrightarrow{F}_{ik}$ from s_k (to repel s_i) are acting simultaneously on s_i. In the case of setting distance threshold as the summation of two sensing ranges, the virtual force $\overrightarrow{F}_{il}$ from s_l equals zero (no force imposed on s_i by s_l). In addition, we incorporate the boundary force $\overrightarrow{F}_{ib}$ to quantify the virtual force acting on s_i from the monitored boundaries. By boundary forces, we can significantly reduce the unwanted coverage outside the sensing field. As depicted in Fig. 2, the magnitude of $\overrightarrow{F}_{ib}$ should be inversely proportional to the perpendicular distance between s_i and the boundary, and is formulated as $|\overrightarrow{F}_{ib}| = w_b(\frac{1}{d_{ib}})$, where w_b represents the weight measurement for the boundary force. In this work, we regard the boundary force as a type of repulsive force, and use the same value for w_r and w_b. In a rectangular area, boundary forces could be from the four boundaries surrounding the monitoring region. Thus $\overrightarrow{F}_{ib}$ is actually the combined force from all boundaries, where $\overrightarrow{F}_{ib} = \overrightarrow{F}_{ib}^{x_1} + \overrightarrow{F}_{ib}^{x_2} + \overrightarrow{F}_{ib}^{y_1} + \overrightarrow{F}_{ib}^{y_2}$. In Fig. 2, since s_i resides at the center, boundary forces from the four boundaries are equal, leading to a zero $\overrightarrow{F}_{ib}$. Considering all attractive, repulsive, and boundary forces, we have the resultant force $\overrightarrow{F}_i$ exerted on sensor s_i being defined as $\overrightarrow{F}_i = \sum_{j=1, j \neq i}^{k} \overrightarrow{F}_{ij} + \overrightarrow{F}_{ib}$. The determined resultant force $\overrightarrow{F}_i$ then guides s_i to *virtually* move to its next position. Since we adopt the discrete coordination system, the next position for s_i is defined as the closest possible grid point. As illustrated in Fig. 2, given the resultant moving angle θ_i, with respect to the positive x axis in counterclockwise direction, we obtain the actual motion angle θ_i' by approximating $\theta_i' = \frac{\pi}{4} round(\frac{\theta_i}{\pi/4})$. Consequently, sensor s_i moves to grid point 4, shown in Fig. 2, as its next position.

Our EVFA-B mechanism terminates when either the required sensing coverage threshold (c_{th}) is achieved or the maximum number of allowable virtual movements performed by each sensor ($Maxloops$) is reached.

A. Distance Threshold

The distance threshold effectively defines the *desired overlapping degree* of two sensors. For homogeneous sensors, the distance threshold can be made as a global constant. However, for heterogeneous sensors, the value of distance threshold should be designed on per node-pair basis to obtain a similar degree of overlapping under different sensing distances. Specifically, for two sensors with small sensing ranges, the distance threshold should be made smaller than that of two sensors with large sensing distances, in order to

keep reasonably similar overlapping level for the two sensor pairs (couples). Besides sensing ranges, the design of distance threshold also depends on the sensor density. Suppose the monitoring area has size A, and the maximum area size covered by all sensors is A_s, where $A_s = \pi \sum_{i=1}^{k} r_i^2$. Define the maximum possible coverage ratio $\widetilde{a} = \frac{A_s}{A}$. Coverage ratio $\widetilde{a} < 1$ implies the total number of sensors is insufficient to fully cover the monitoring area. In this case, we cannot afford overlapping between sensors. On the other hand, coverage ratio $\widetilde{a} \geq 1$ indicates the sensor population is capable of fully covering the whole area, in which case a certain degree of overlapping is desirable to minimize the sensing holes (uncovered zones). Based on the above principles, we propose to separately design the distance threshold d_{th}^{ij} for any two sensors s_i and s_j under four environmental settings. For homogeneous sensors, we use the abbreviation ISR to reflect the fact of having Identical Sensing Radius. For heterogeneous sensors, we use HSR to represent the condition of possessing Heterogeneous Sensing Ranges. As illustrated in Fig. 3(a), **Case I** and **Case III** deal with insufficient sensor population (reflected by $\widetilde{a} < 1$) for homogeneous and heterogeneous sensors respectively, where overlapping is not desirable. As a result, the distance threshold is simply designed as the sum of two sensing ranges. In **Case II** and **Case IV**, where sensor population is sufficient to allow overlapping (due to $\widetilde{a} \geq 1$), the design of distance threshold should try to minimize the sensing holes. In **Case II**, it is easy to obtain the perfect (minimum) overlapping by setting $d_{th}^{ij} = 2r \cos(\pi/6)$, while in **Case IV**, we set $d_{th}^{ij} = \alpha(r_i + r_j)$ by introducing a system-tunable factor α to control the desired overlapping degree, where $0 < \alpha < 1$. Consequently, we have the distance threshold d_{th}^{ij} being formulated in our model as

$$d_{th}^{ij} = \left\{ \begin{array}{ll} 2r & \text{for } \textbf{ISR} \text{ with } \widetilde{a} < 1 \\ 2r \cos(\frac{\pi}{6}) & \text{for } \textbf{ISR} \text{ with } \widetilde{a} \geq 1 \\ r_i + r_j & \text{for } \textbf{HSR} \text{ with } \widetilde{a} < 1 \\ \alpha(r_i + r_j) & \text{for } \textbf{HSR} \text{ with } \widetilde{a} \geq 1 \end{array} \right\}. \quad (2)$$

B. Weight Constants

For the self-deployment algorithm based on virtual forces to perform effectively in achieving high sensing coverage in a bounded $m \times n$ area, the design of weight constants w_a and w_r associated with the attractive and repulsive forces is a critical issue. Intuitively, w_r should be set much larger than w_a (as suggested in [18]), considering the relatively small number of neighboring sensors (exerting repulsive forces) compared to the large number of non-neighboring nodes out there (exerting attractive forces). However, experimental experiences reveal that arbitrary settings of a large w_r and a small w_a do not produce effective sensing coverage in many cases. In this section, we attempt to characterize the relationship between w_r and w_a by deriving a *better formulated equation* for setting the two weight constants than simply suggesting to use $w_r >> w_a$ (with arbitrary settings).

Consider an extreme node configuration shown in Fig. 3(b), where all the sensors (except for s_i and s_j) are located in one corner of the $m \times n$ sensing field. For sensor s_i, the virtual forces it receives include the repulsive force from s_j
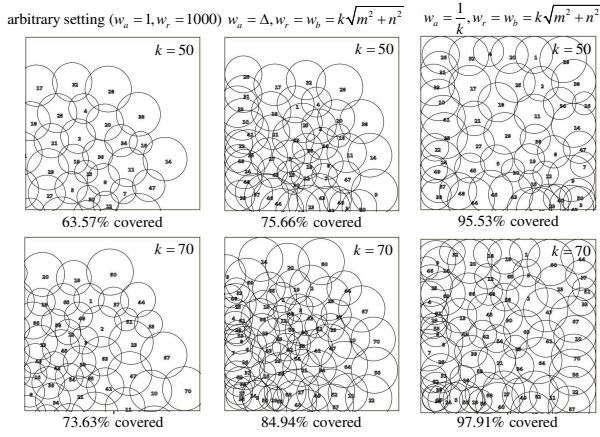
Fig. 4. Impact of w_a, w_r $(= w_b)$ parameter settings on the coverage ratio of monitored 200×200 area (HSR with $\tilde{a} \geq 1$).

and attractive forces from all the other $(k-2)$ nodes. The magnitude of repulsive force from s_j is denoted as $|\overrightarrow{F}_i^R|$. Based on the definition of repulsive force provided in Eq. (1), we have $|\overrightarrow{F}_i^R| = w_r|d_{th}^{ij} - d_{ij}| = w_r\Delta$, where Δ is a small value that represents the *tolerable overlapping* between s_i and s_j. On the other hand, since the average distance between s_i and all the other $(k-2)$ nodes is approximately $(\sqrt{m^2 + n^2} - \sqrt{2}r_i - \sqrt{2}r_k)$, the magnitude of total attractive forces acting on s_i is given by $|\overrightarrow{F}_i^A| = (k-2)w_a(\sqrt{m^2 + n^2} - \sqrt{2}(r_i + r_k))$. Due to the relatively small values of r_i and r_k compared to the area dimensions (m and n), we neglect the term $\sqrt{2}(r_i + r_k)$. Moreover, by approximating $(k-2) \approx k$, we have $|\overrightarrow{F}_i^A| = w_a k\sqrt{m^2 + n^2}$. $\overrightarrow{F}_i^R$ and $\overrightarrow{F}_i^A$ are two forces that drive sensor s_i toward the opposite directions. To keep s_i in a balanced state without being drawn toward the center or pushed outside the sensing field, we adopt the equality of the two forces by making $|\overrightarrow{F}_i^R| = |\overrightarrow{F}_i^A|$. Consequently, we have $\frac{w_r}{w_a} = \frac{k\sqrt{m^2 + n^2}}{\Delta}$, where m, n, and k are environmental constants, while Δ $(= |d_{th}^{ij} - d_{ij}|)$ varies with the tolerable overlapping degree of respective sensor pair (related to the sensing ranges and resultant d_{th}^{ij}). Based on the above derivations, proper choices for the weight constants can be made by setting $w_r = k\sqrt{m^2 + n^2}$ and $w_a = \Delta$.

Next, we intend to further relax w_a from the dependency on sensing radius by considering setting w_a inversely proportional to the sensor population k as another alternative to the positive (attractive) weight value. In the case of having a large sensor population (with large k), the weight associated with the positive force should be made small to avoid exerting too much total attractive force on a sensor, and vice versa. To maintain a balanced force interaction, it is reasonable to relate the attractive weight measurement to the actual sensor population (parameter k). As a result, we propose another alternative to proper weight choices by setting $w_r = k\sqrt{m^2 + n^2}$ and $w_a = \frac{1}{k}$.

In addition, since the monitored environment is usually in a bounded area, we also incorporate the boundary forces (with weight constant w_b) in our EVFA-B mechanism. We use the same value for w_r and w_b, considering the boundary force is also a kind of repulsive force. In Fig. 4, we perform EVFA-B
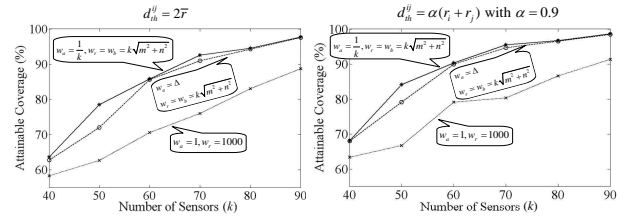

Fig. 5. Performance justification of proper choices for $d_{th}^{ij}, w_a, w_r(w_b)$ values in our EVFA-B algorithm.

(with $Maxloops = 100$, $c_{th} = 0.95$, $\alpha = 0.9$) and experiment on two sensor populations ($k = 50$ and $k = 70$) under three different settings of w_r and w_a as discussed earlier. As we can see from the figure, arbitrary setting (though $w_r >> w_a$) without boundary forces performs poorly, while the third alternative by making w_a inversely proportional to k performs the best with the highest coverage ratio achieved. Interestingly, by setting $w_a = \frac{1}{k}$ (independent of sensing radius), we actually obtain a better sensing coverage than that by setting $w_a = \Delta$ (sensing radius dependent), which implies that *good choices for the weight constants depend on the sensor population (parameter k) and monitoring dimensions (m and n), and can be made independent of sensing radius*. This implication greatly simplifies the design of weight constants when dealing with heterogeneous sensors (having varying sensing ranges). Therefore we adopt the third alternative by setting $w_r = k\sqrt{m^2 + n^2}$ and $w_a = \frac{1}{k}$ in our EVFA-B mechanism thereafter.

C. Verification of Parameter Settings

We conduct more EVFA-B experiments ($Maxloops = 100$, $c_{th} = 0.95$) in this section to observe the combined impact of d_{th}^{ij}, w_a, w_r settings on the attainable coverage ratio. In Fig. 5, two d_{th}^{ij} designs are experimented (where $\bar{r} = \frac{1}{k}\sum_{i=1}^{k} r_i$, representing the average sensing radius), both with three different w_a, w_r settings. As depicted in the figure, by setting $w_a = \frac{1}{k}$ and $w_r = k\sqrt{m^2 + n^2}$, we obtain the highest coverage under both d_{th}^{ij} values. Moreover, even higher coverage ratio is attainable if we make the distance threshold on per node-pair basis by setting $d_{th}^{ij} = \alpha(r_i + r_j)$. The results indicate the importance of proper parameter settings on the distance threshold (d_{th}^{ij}) and weight constants (w_a, w_r, w_b), further validating our parameter designs proposed in Section IV-A and Section IV-B.

D. EVFA-B Algorithm Summary

Table I summarizes the notations used in the EVFA-B mechanism, and Algorithm 1 provides the pseudocode for EVFA-B operations. Note that in the end of each loop, every sensor performs *virtual movement* without physically moving to the new position. Physical movements are conducted once the EVFA-B process terminates (either c_{th} or $Maxloops$ has been reached).

V. PERFORMANCE EVALUATION

In this section, we validate the proposed EVFA-B protocol by comparing the performance with two other self-deployment

TABLE I
SUMMARY OF NOTATIONS USED IN OUR EVFA-B

Notation	Description
m	Length of the monitored field
n	Width (breadth) of the monitored field
k	Total number of sensor nodes (denoted as $s_1, s_2, \cdots, s_k$ with radius $r_1, r_2, \cdots, r_k$)
(x_i, y_i)	Coordinate (position) of sensor s_i
d_{th}^{ij}	Distance threshold for two arbitrary sensors s_i and s_j ($j \neq i$)
w_a	Tunable weight measure for attractive force
$w_r (w_b)$	Tunable weight measure for repulsive force (boundary force)
$\overrightarrow{F_i}$	Resultant force exerted on sensor s_i (attractive, repulsive, boundary forces considered)
$Maxloops$	Maximum number of virtual movements performed by each sensor
c_{th}	Desired coverage ratio threshold

Algorithm 1 EVFA-B Procedures

1: set $loops = 0$;
2: set $c_{now} = c_{init}$; // initial coverage ratio
3: **while** ($loops < Maxloops$) && ($c_{now} < c_{th}$) **do**
4:     **for** each sensor $s_i \in \{s_1, s_2, ..., s_k\}$ **do**
5:         compute $\overrightarrow{F}_i = \sum_{j \neq i, j=1}^{k} \overrightarrow{F}_{ij} + \overrightarrow{F}_{ib}$;
6:     perform *virtual movements*; // all sensors virtually move to their next positions
7:     update *coverage ratio* c_{now};
8:     set $loops = loops + 1$;

mechanisms in terms of coverage ratio and total energy consumed by sensor physical movements. The comparison targets include mechanisms also based on virtual forces. We implement Zou (introduced in [18]) and Zou-B (improved Zou mechanism by incorporating boundary forces into the force calculations) with fixed weight settings. Since there is no specific design guidelines provided by [18] on setting the weights except for suggesting to use $w_r >> w_a$, we try on several w_r and w_a combinations and select ($w_a = 1, w_r = 1000$) to be utilized by Zou and Zou-B for its best coverage performance. On the other hand, the weight settings in EVFA-B follow the derivations presented in Section IV-B and are made as ($w_a = \frac{1}{k}, w_r = k\sqrt{m^2 + n^2}$). For the weight w_b associated with the boundary force (considered by both EVFA-B and Zou-B), we use the same value set for w_r (i.e., $w_b = w_r = k\sqrt{m^2 + n^2}$ in EVFA-B and $w_b = w_r = 1000$ in Zou-B). We simulate heterogeneous sensors, having sensing radius uniformly distributed in $[10, 20]$, in a rectangular grid-based region. The distance threshold in Zou and Zou-B is set as twice the average sensing radius (i.e., $d_{th}^{ij} = 2\overline{r}$, where $\overline{r} = \frac{1}{k}\sum_{i=1}^{k} r_i$), while EVFA-B follows Eq. (2) on setting the threshold (with overlapping factor $\alpha = 0.9$). All three mechanisms use $Maxloops = 100$ and $c_{th} = 0.95$ as their deployment termination conditions.

A. Improved Surveillance Coverage

Fig. 6 displays the deployment results accomplished by Zou, Zou-B, and EVFA-B respectively at the 50th round, halfway to the maximum allowable loops of 100. We observe that, given the same computation time, EVFA-B is able to make the most effective progress toward the required sensing coverage. On the other hand, due to lack of boundary forces, Zou makes many unnecessary movements outside the sensing field.
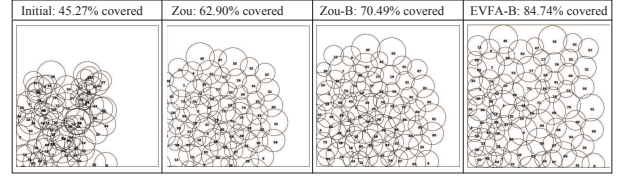

Fig. 6. Sensor deployment status after 50 rounds (virtual movements) using Zou, Zou-B, and our proposed EVFA-B strategies, respectively ($m = 200, n = 200, k = 80$, HSR with $\widetilde{a} \geq 1$).
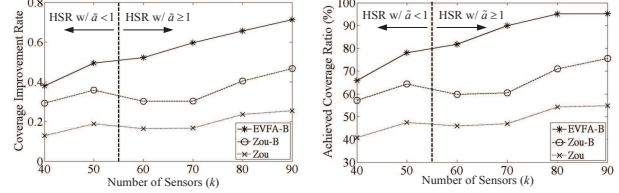

Fig. 7. Coverage performance accomplished by Zou, Zou-B, and our EVFA-B deployment strategies under various amounts of sensor nodes in a monitored 200×200 area.

By incorporating the boundary forces to keep sensors from drifting away, Zou-B outperforms Zou as a result of reducing unwanted coverage outside the monitoring region. However, due to improper distance threshold and weight settings, Zou-B is unable to cover the area as effectively as EVFA-B does.

The results in Fig. 6 motivate us to conduct another set of experiments investigating the *coverage improvement rate* of respective mechanism under different environmental settings. We define the coverage improvement rate as the *average amount of coverage ratio improved/increased per round/loop*, regarded as the progressing speed on enhancing sensing coverage. Since the three mechanisms have different progressing speeds, intuitively, the one with the highest coverage improvement rate is expected to produce the best coverage ratio. We experiment on various sensor populations in the same monitoring region as Fig. 6 to observe the coverage improvement rate and achieved coverage ratio. As shown in Fig. 7, after the first redeployment, EVFA-B achieves the best sensing coverage due to its highest coverage improvement rate under all sensor populations. Moreover, we observe that both the coverage improvement rate and achieved coverage ratio of EVFA-B increase monotonically as number of sensors grows. The reason is attributed to the judicious designs of distance threshold and weight constants, making the deployment strategy adopted by EVFA-B adaptive to environmental parameters (such as sensor numbers, area dimensions, and heterogeneous sensing ranges). On the other hand, Zou and Zou-B do not have steadily increasing performance as sensor population grows, due to their improper parameter designs, making the two mechanisms incapable of utilizing the benefit brought by increased number of deployable sensors.

B. Energy Conservation on Physical Movements

Due to the centralized computations and communications exercised by Zou, Zou-B, and EVFA-B, the major source of energy consumption is from sensor physical movements. To model the energy consumed by the motion device moving for
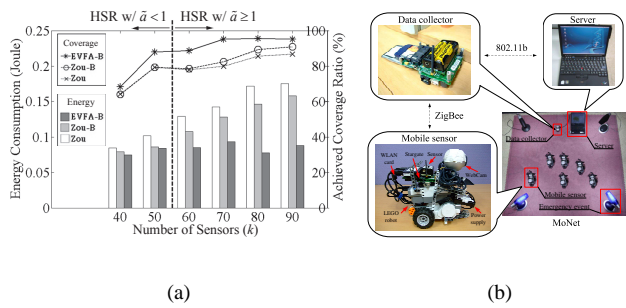
Fig. 8. (a) Physical movement energy consumption comparison after the first redeployment is respectively completed by Zou, Zou-B, and EVFA-B under various amounts of sensor nodes in a monitored 200×200 area. (b) Validation of the proposed EVFA-B protocol by implementing a real-world monitoring network (MoNet) via commodity hardware components.

one grid unit, we do real measurements on the sensor robot used in our implementation testbed with grid size equal to 1 cm. The robot assembles six 1.2 V 2000 mAh rechargeable NiMH batteries with measured $200 \sim 290$ mA moving current and average moving speed at 0.06 m/sec (216 m/hr). Consequently, the average moving energy consumption per grid (unit distance) can be estimated by $0.29 \times 7.2 \times (\frac{0.01}{216}) = 9.667 \times 10^{-5}$ Joule. We obtain the total energy consumed by physical movements performed by respective deployment strategy based on the estimated energy model, and conduct experiments to observe the energy performance under different sensor populations. Fig. 8(a) shows the results of both energy consumption and achieved coverage ratio. EVFA-B yields the highest coverage ratio, while consuming the least energy on physical movements, due to its capability of keeping sensors from moving far away. The results indicate that EVFA-B is both coverage effective and energy efficient, which encourages us to implement the EVFA-B protocol in a practical testbed.

C. Implementation of MoNet Prototype

As pointed out in [7] that simulation models do not sufficiently capture the radio and sensor irregularity in a real-world environment, a proof-of-concept implementation is thus needed to demonstrate the feasibility of our proposed EVFA-B protocol. In this section, we briefly report our prototyping experiences on an automated monitoring network (MoNet).

Fig. 8(b) illustrates the hardware architecture and communication protocols used by our MoNet. the mobile sensor is basically a moving robot (LEGO MINDSTORMS NXT 9797 [2]) carrying a single-board computer (Crossbow Stargate [1]), a sensor-equipped mote (Crossbow MICAz [1]), and a webcam device (Logitech QuickCam Pro 4000 [3]). The server acts as the clusterhead performing deployment-related computations required by EVFA-B, while the data collector is responsible for gathering necessary data (such as sensor locations and sensing ranges) from all sensors via ZigBee protocol and providing them to the server. In our testbed, the location information is obtained via a pre-deployed RFID positioning system with grid granularity of 1 cm. To demonstrate the emergency response capability of MoNet, we randomly place six mobile sensors in a $2m \times 2m$ area, and generate four emergency events (using desk lamps instead of real fire for safety concerns) at the

four corners. We configure the sensors to regard a light event with reading above 900 as an abnormal event (emergency) and report the detected event back to the server upon the detection. A demonstration video on this experiment is available in [4].

VI. CONCLUSION

In this paper, we proposed an enhanced sensor deployment protocol, entitled EVFA-B, with the objective of providing sufficient surveillance coverage for smart indoor environments. In the development of EVFA-B, distance threshold settings and weight constants (associated with attractive/repulsive forces) have been judiciously designed to effectively increase the sensing coverage ratio. Performance results showed that EVFA-B outperformed other virtual forces algorithms due to its better parameter choices and the incorporation of virtual boundary forces. Furthermore, an automated monitoring network (MoNet) powered by our EVFA-B deployment mechanism was implemented as a proof-of-concept prototype to corroborate the protocol feasibility.

REFERENCES

[1] Crossbow Technology. http://www.xbow.com/.
[2] LEGO MINDSTORMS. http://www.lego.com/en-US/default.aspx.
[3] Logitech QuickCam Pro 4000. http://www.logitech.com/.
[4] MoNet Video. http://bunlab.twbbs.org/filezone/files/EVFA-B.mpg.
[5] S. S. Dhillon and K. Chakrabarty. "Sensor Placement for Effective Coverage and Surveillance in Distributed Sensor Networks". *In Proc. IEEE WCNC*, pages 1609–1614, March 2003.
[6] A. Howard, M. J. Mataric, and G. S. Sukhatme. "Mobile Sensor Network Deployment Using Potential Fields: A Distributed Scalable Solution to the Area Coverage Problem". *In Proc. Int'l Symposium on Distributed Autonomous Robotics Systems*, June 2002.
[7] D. Johnson, T. Stack, R. Fish, D. M. Flickinger, L. Stoller, R. Ricci, and J. Lepreau. "Mobile Emulab: A Robotic Wireless and Sensor Network Testbed". *In Proc. IEEE INFOCOM*, April 2006.
[8] F. Y. S. Lin and P. L. Chiu. "A Near-optimal Sensor Placement Algorithm to Achieve Complete Coverage/Discrimination in Sensor Networks". *IEEE Communications Letters*, 9(1):43–45, January 2005.
[9] J. Lu and T. Suda. "Differentiated Surveillance for Static and Random Mobile Sensor Networks". *IEEE Transactions on Wireless Communications*, 7(11):4411–4423, November 2008.
[10] A. Mainwaring, J. Polastre, R. Szewczyk, D. Culler, and J. Anderson. "Wireless Sensor Networks for Habitat Monitoring". *In Proc. Int'l Workshop on Wireless Sensor Networks and Applications (WSNA)*, 2002.
[11] S. A. Musman, P. E. Lehner, and C. Elsaesser. "Sensor Planning for Elusive Targets". *Elsevier Mathematical and Computer Modelling*, 25(3):103–115, February 1997.
[12] K.-H. Peng, T.-Y. Lin, and K.-H. Chen. "On Seamless Wireless Sensor Deployment and System Implementation". *Int'l Journal of Advanced Information Technologies (IJAIT)*, 3(2):72–92, December 2009.
[13] O. Tekdas, V. Isler, J. H. Lim, and A. Terzis. "Using Mobile Robots to Harvest Data from Sensor Fields". *IEEE Wireless Communications*, February 2009.
[14] G. Wang, G. Cao, and Thomas F. La Porta. "Movement-assisted Sensor Deployment". *IEEE Transactions on Mobile Computing*, 5(6):640–652, June 2006.
[15] X. Wang, G. Xing, Y. Zhang, C. Lu, R. Pless, and C. Gill. "Integrated Coverage and Connectivity Configuration in Wireless Sensor Networks". *In Proc. ACM Sensys*, November 2003.
[16] J. Wu and S. Yang. "SMART: A Scan-based Movement-assisted Sensor Deployment Method in Wireless Sensor Networks". *In Proc. IEEE INFOCOM*, March 2005.
[17] H. Zhang and J. C. Hou. "Maintaining Sensing Coverage and Connectivity in Large Sensor Networks". *Ad Hoc and Sensor Wireless Networks*, 1(1-2):89–124, March 2005.
[18] Y. Zou and K. Chakrabarty. "Sensor Deployment and Target Localization Based on Virtual Forces". *In Proc. IEEE INFOCOM*, April 2003.